OPEN ACCESS

University of BRISTOL

Peer reviewed version

Link to published version (if available):
10.1016/j.jpurol.2018.12.004

Link to publication record in Explore Bristol Research
PDF-document

University of Bristol - Explore Bristol Research

General rights

1   **Functional, histological and molecular characteristics of human exstrophy detrusor**

2

3   **N Johal[1], C Arthurs[2,4], P Cuckow[1], K Cao[2,4], DN Wood[3], A Ahmed[4], CH Fry[2]**

4   1. Department of Urology, Great Ormond St Hospital for Sick Children, London UK

5   2. School of Physiology, Pharmacology & Neuroscience, University of Bristol, UK

6   3. Department of Urology, University College Hospitals, London, UK

7   4. Centre for Stem Cells and Regenerative Medicine, King's College London, UK

8

9   **Corresponding author**

10   **CH Fry,** School of Physiology, Pharmacology & Neuroscience, University Walk, University of Bristol,

11   Bristol BS8 1TD, UK

12   chris.fry@bristol.ac.uk

13

14

15

16   **Short title:** Pathophysiology of human exstrophy detrusor

17

18   **Extended summary**

19   *Introduction*. Bladder exstrophy is a congenital anomaly involving fetal exposure and protrusion of

20   the open bladder through an incomplete lower abdominal wall. Techniques to surgically correct

21   exstrophy after birth have greatly improved, but it still presents a major challenge to achieving

22   continence and a good quality of life for patients and their families as the pathophysiology of

23   bladder dysfunction is unknown.

24   *Objectives.* A multimodal approach was used to characterise the histological and biomechanical

25   properties of exstrophy detrusor. These were correlated with myocyte responses to agonists and

26   an evaluation of developmental signalling pathways to evaluate the cause of bladder dysfunction in

27   exstrophy.

28   *Study design*. Detrusor muscle specimens were obtained during corrective surgery from four

29   exstrophy groups: neonatal (1-3 days, *n*=8), younger children (7months-5 years, *n*=13) and older

30   children (8-14 years, *n*=11) undergoing secondary procedures and cloacal exstrophy (16 days-9

31   years, *n*=9); control specimens were obtained from children (3 months-9 years, *n*=14) undergoing

32   surgery for other pathologies but with normal bladder function. Five lines of experiments were

33   undertaken: measurement of connective tissue to detrusor muscle ratio, contractile responses to

34   electrical and agonist stimulation; *in vitro* biomechanical stiffness, intracellular Ca^{2+} responses to

35   contractile agonists and immunohistochemistry for proteins (MMP-7, cyclinD1, ß-catenin and *c-*

36   *myc*) involved in fibrosis generation. Exstrophy data were compared to those from the control

37   group.

38   *Results*. Exstrophy tissue demonstrated reduced smooth muscle compared to connective tissue,

39   reduced contractile responses and greater mechanical stiffness. However, intracellular Ca^{2+}

40   responses to agonists were maintained. These changes were greatest in neonatal and cloacal

41   exstrophy samples and least in those from older paediatric bladders. Immunolabelled MMP-7, ß-

42   catenin and *c-myc* were reduced in exstrophy samples.

43　*Discussion.*　These results highlight the reality that newborns with exstrophy have significantly

44　reduced compliance and bladder underactivity, which may persist or return to normal values with

45　surgery and age. The primary cause of underactivity is increased connective tissue in relation to

46　detrusor muscle, however detrusor myocyte function remains normal. Finally, the increase of

47　smooth muscle content in the paediatric bladder group indicates a remodelling response of the

48　bladder to surgical correction and time. Excess gestational fibrosis is associated with changed

49　expression of key proteins in the *Wnt*-signalling pathway, a potential aetiological factor and

50　therapeutic target.

51　*Conclusion.* Results point to connective tissue deposition as the primary pathological process that

52　determines bladder function with normal myocyte function. Future research that reduces

53　connective tissue deposition may lead to improvement in outcomes for these children.
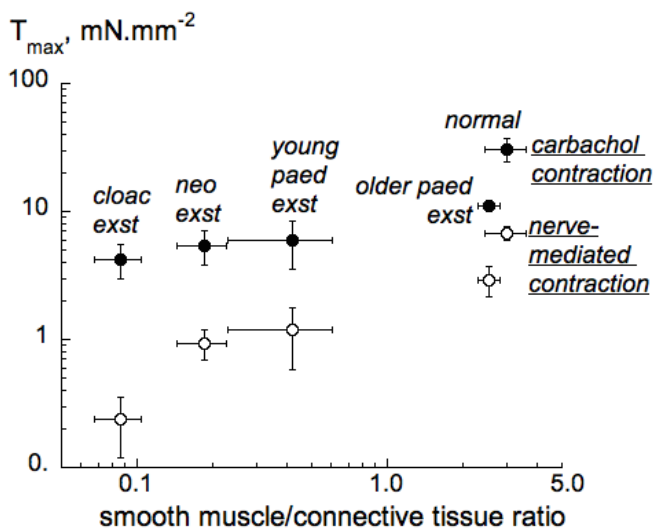
54

Introduction

Bladder exstrophy is part of the exstrophy-epispadias complex whereby developmental failure of the lower abdominal wall *in utero* leads to a bladder that remains pathologically open and protruding: the prevalence is 3 per 100,000 live births [1]. After neonatal closure, further reconstructive surgery achieves continence, and functional and cosmetically acceptable genitalia. The Kelly procedure [2] is performed at Great Ormond Street Hospital for Children, but in other specialist centres, single and staged-repair techniques are used. Despite successful reconstruction many patients continue with low-capacity bladders with insufficient contractile function [3,4], although a retrospective review of 13 patients following complete primary repair showed good functional recovery [5].

Characteristic of bladder exstrophy [6,7] is increased bladder wall collagen and denervation [8]. Increased collagen results from transformation of several cell types, particularly fibroblasts and epithelia, into myofibroblasts [9]; as well as reduced matrix metalloproteinase (MMP) expression and enhanced expression of tissue inhibitor of metalloproteinases (TIMP) [10]. These processes are controlled by transforming growth factor-β (TGF-β) and augmented by release of *Wnt*-ligand proteins to promote myofibroblast differentiation [11], mediated by transcription factors such as β-catenin, c-*myc* and cyclin-D1. Massive parallel sequencing identified coding changes in 50% of exstrophy patients in 19 different *Wnt* genes [12]. However, functional characterisation to support histological and genetic changes is sparse. In this study, we measured contractile and biomechanical properties of detrusor smooth muscle from human exstrophy bladders and characterised changes to the *Wnt*-signalling pathway to identify potential pathways that may be therapeutic targets to reverse associated fibrosis. We tested the hypothesis that more connective tissue at the expense of smooth muscle in the exstrophy bladder is associated with reduced contractile performance and greater biomechanical stiffness, and if the former was associated with functional denervation and

80   smooth muscle failure. We carried out experiments *in vitro* with isolated detrusor samples to

81   measure: smooth muscle and connective tissue content; active force generation; passive stiffness

82   and intracellular Ca^{2+} responses to contractile agonists. We also performed preliminary

83   observations regarding the molecular basis of increased connective tissue deposition by measuring

84   any changes to the *Wnt*-signalling pathway.

85

86   **Methods**

87   *Tissue samples, ethics and preparations*. Bladder biopsy samples came from five patient groups. A

88   control group ($n=14$; 10 male (M), 4 female (F); 3 months-9 years) with normal bladder function

89   undergoing open bladder surgery (ureteric reimplantation, urachal cyst excision, localised tumour

90   excision). Four exstrophy groups: i) neonatal exstrophy at time of primary bladder closure ($n=8$; 6M,

91   2F; age 1-3 days); ii) cloacal exstrophy ($n=9$; 3M, 6F; 16 days-9 years); iii) young children receiving

92   secondary procedures ($n=13$; 8M, 5F; 7months-5 years): a Kelly soft tissue reconstruction ($n=10$),

93   redo bladder neck repair with augmentation ($n=1$), bladder neck closure with augmentation ($n=1$)

94   and bladder and abdominal wall closure for covered variant exstrophy ($n=1$); iv) older children

95   receiving secondary procedures ($n=11$; 8M, 3F; 8-14 years) by Kelly repair ($n=3$), bladder neck repair

96   with augmentation ($n=6$) or bladder neck closure ($n=2$).

97   All samples were from the lateral wall of the bladder dome, with no evidence of adjacent metaplasia

98   in the one case of tumour excision. After ethical approval, the study was accepted by the R&D

99   department, Great Ormond Street Hospital, London, UK. Parents or guardians were given an

100   information sheet and consent obtained at least 24 hours later. Samples were carried in Ca^{2+}-free

101   solution, within 1-2 hours, to the laboratory for immediate use. Serosa and mucosa were removed

102   by blunt dissection, and detrusor strips (1 mm diam; 4-5 mm length) dissected.

103   *Solutions.* Functional experiments (36°C) in Tyrode's solution (mM): NaCl, 118; $NaHCO_3$, 24; KCl,

104   4.0; $MgCl_2$, 1.0; NaH_2PO_4, 0.4; $CaCl_2$, 1.8; glucose, 6.1; Na pyruvate, 5.0; pH 7.4, 5%CO_2,95% O_2.

105   Ca^{2+}-free solution was (mM): NaCl, 132; KCl, 4.0; NaH_2PO_4, 0.4; glucose, 6.1; Na pyruvate, 5.0;

106   HEPES, 10.0, pH 7.4 with 1M NaOH. High-K Tyrode's contained 80 mM KCl, with no osmolality

107   correction. Drugs were diluted from aqueous stocks. Cell isolation used Ca^{2+}-free solution plus

108   (mg/ml): Worthington Type-II collagenase, 20; hyaluronidase-IS, 0.5; hyaluronidase-III, 0.5;

109   antitrypsin-IIS, 0.9; bovine albumin, 5.0 [13]. All chemicals were from Sigma UK.

Active tension recording. Muscle strips were tied in a horizontal superfusion trough between an isometric force transducer and a fixed hook. Nerve-mediated contractions were elicited by electrical field stimulation (3-s trains, width 0.1ms, frequency 1-40Hz); abolished by 1μM tetrodotoxin. Contractions generated by direct muscle stimulation were elicited by the muscarinic agonist carbachol (0.1-30μM) or the purinergic agonist α,β–methylene ATP (ABMA, 10 μM). The peak increase from baseline tension was recorded and normalised to cross-section area, *a*.

Biomechanical experiments. Muscle strips were tied between the force transducer and the central pole of a rotary solenoid. Application of a step voltage to the solenoid rotated it to stretch the muscle by up to 1 mm (20% resting length, *L,* i.e. $\Delta L/L = 0.2$) for 50 s before returning to the original length. Stretches were in triplicate at 5-min intervals and average values used. Upon stretch tension, *T*, increased followed by partial relaxation (magnitude T_2, time constant τ), to a new steady-state value, T_1 (figure 3A). The elastic modulus, *E*, was calculated from $E = T_1/(a*\Delta L/L)$; units megapascal, MPa=1N.mm^{-2}). Tension (and hence elastic modulus) immediately after a stretch was greater, the component dissipated by viscoelastic relaxation was calculated by $E_2 = T_2/(a*\Delta L/L)$.

Measurement of intracellular Ca^{2+}, [Ca^{2+}]$_i$. Small (1 mm^3) biopsy pieces were gently triturated for up to 20 min in 1ml of cell isolation solution, gently centrifuged, the supernatant decanted and replaced with Tyrode's solution. The Ca^{2+} fluorochrome Fura-2 (5 μM) was added for 20-30 minutes. Myocytes were identified by a spindle-shaped appearance and samples fixed in 4% formalin solution and labelled for smooth-muscle myosin for confirmation. A drop of cell suspension was placed in a heated (36°C) superfusion chamber and [Ca^{2+}]$_i$ measured by alternate (32 Hz) excitation at 340 and 380 nm; fluorescent light was collected between 410 and 510 nm. The magnitude of the fluorescence ratio measured at 340 and 380nm excitation, $R_{340/380}$, was a function of [Ca^{2+}]$_i$. The system was calibrated as described previously [13].

133   *Histology*. Portions of the biopsy were placed in 10 % formaldehyde and stored at 4°C. Samples

134   were dehydrated in alcohol, then xylene and paraffin. Sections (5 μm) on TESPA-coated glass slides

135   were stained with Elastin van Gieson (collagen, red; elastin, black; muscle yellow/orange). The

136   proportion of muscle to connective tissue (collagen and elastin) was measured using colour filters

137   on Image-J. Three separate regions (50x50 μm) per section were measured, distant from mucosa or

138   any obvious areas absent of tissue, and the average recorded.

139   *Multi-channel immunofluorescence labelling and quantitative image intensity analyses.* Antibodies

140   for MMP7 (Abcam), cyclin-D1 (Santa Cruz), ß-catenin and *c-myc* (Novacastra/Leica) were optimised

141   for concentration, pH-dependence and antigen retrieval. A Bond maX™ automated system (Leica

142   BioSystems) was used for labelling [14], the researcher was blind to the antibodies used. Antibodies

143   were incubated simultaneously on each section and labelled with secondary fluorescent antibodies;

144   Cy3 (514/565 nm), Cy5 (633/671 nm), FITC (488/517 nm), Cy3.5 (561/617 nm) respectively, as well

145   as the nuclear counter-stain DAPI (405/429 nm). Each section was imaged with a TCS SP8 confocal

146   system (Leica) at 20x (dry objective) and 40x (1.3 NA, oil objective) with a 6x digital zoom and a *z*-

147   step of 0.17μm. High magnification (x63) images were taken from three, randomly selected, areas

148   of each section and analysed using Huygens professional image deconvolution software (Scientific

149   Volume Imaging, Hilversum, NL) [14] using a macro compiled to measure individual intensities.

150   *Data presentation and analysis.* Data are mean±SEM, *N;n*=number of biopsies;preparations.

151   Immunofluorescence data are medians [25,75% interquartiles] as sets were not normally

152   distributed. Significances between multiple data sets used parametric or non-parametric ANOVA,

153   followed by appropriate *post hoc* tests; the null hypothesis was rejected at *$p<0.05$, **$p<0.01$,

154   ***$p<0.001$. Dose-response or force-frequency curves were fitted to: $T=(T_{max}.x_m)/(x_m+k_m)$; where

155   T_{max} is the maximum response at high stimulation frequency (*f*) or agonist concentration (*S*); *x* is the

156   different values of *f* or *S*; k_m is the value of *x* required to achieve $T_{max}/2$; *m* is a constant. A Spearman

157   correlation coefficient, *r*, tested associations between two variables, for subsequent estimation of

158   a *p*-value.

159

160   **Results**

161   *Histology measurements.* Figure 1A shows sample sections of detrusor from control and young

162   paediatric exstrophy patients, the latter shows mucosa on the left edge which was avoided for

163   analysis. The ratio of smooth muscle to connective tissue (SM/CT) was measured for all five groups.

164   In all exstrophy cohorts, except the older paediatric cohort, the SM/CT ratio was significantly lower

165   compared to the normal cohort (Table 1). Moreover, there was a progressive and significant decline

166   of the ratio from the control and older paediatric exstrophy groups, through to younger paediatric

167   exstrophy, neonatal and cloacal exstrophy groups (figure 1B).

168   *Contractile responses to nerve-mediated and agonist-induced activation.* The frequency-

169   dependence of nerve-mediated contractions from normal and exstrophy bladders was used to

170   determine: maximum tension at high frequencies, $T_{max,n-m}$, and $f_{1/2}$, the frequency that generates

171    $T_{max,n-m}/2$ (figure 2A). $T_{max, n-m}$ was reduced in both paediatric, neonatal and cloacal exstrophy

172   groups compared to control; $f_{1/2}$ values were similar in all groups (Table 1). Atropine-resistance, the

173   percentage residual tension after 1µM atropine, was present in all groups (Table 1, not determined

174   in cloacal exstrophy); percentage values were highly variable, with no significant differences

175   between the cohorts, but in all the data were significantly different from zero.

176   Dose-response curves to the muscarinic agonist, carbachol showed that the maximum response

177   ($T_{max,carb}$) was lower in all four exstrophy groups. However, carbachol potency was greater in both

178   paediatric and the neonatal exstrophy groups, as seen by larger pEC_{50} values (Table 1), statistical

179   analyses were not performed for agonist data from the cloacal exstrophy group, due to the small

180   sample number. A similar pattern was observed in the magnitude of responses to a single

181   concentration (10 µM) of ABMA. Finally, the ratio of the maximum responses to nerve-mediated

182   stimulation and carbachol ($T_{max,n-m}/T_{max,carb}$) was calculated: a smaller ratio is interpreted as reduced

183   functional innervation; values were similar in all five groups (Table 1). The relationships between

184   maximum response to nerve-mediated stimulation (closed circles) or carbachol (open circles) as a

185   function of the SM/CT ratio are shown in figure 2B; contraction magnitude diminished as smooth

186   muscle content decreased.

187   *Passive biomechanical properties*. The transient and steady-state passive tensile properties of

188   detrusor muscle strips were measured during a 50s stretch by 20% of the resting length ($\Delta L/L$=0.2).

189   Three variables were measured: steady-state tension (T_1, N.mm^{-2}); magnitude of viscoelastic

190   relaxation (T_2, N.mm^{-2}) and the time constant of viscoelastic relaxation (τ, s; figure 3A, Table 2).

191   Three stretches, five minutes apart, were applied; T_1 and T_2 values were significantly greater during

192   the second and third stretches and similar in value to each other; values of τ were similar for all

193   three stretches. Average values from the second and third stretches for each variable are quoted.

194   Measurements from detrusor samples of control, paediatric exstrophy and neonatal exstrophy

195   bladders were made. Data from the older and young paediatric exstrophy groups were combined

196   due to the relatively small number of biopsy samples tested. No data were available for cloacal

197   exstrophy bladders as the biopsy samples were too small.

198   The value of elastic modulus, E, a steady-state measure of tissue stiffness, was calculated from T_1

199   values (see Methods). Values of T_1, for the control, paediatric and neonatal exstrophy groups are

200   shown in figure 3B. Exstrophy data were significantly greater than compared to the normal group.

201   T_2 values were smaller than T_1 in all samples, but a similar trend was measured as for T_1 in the

202   three groups: values of τ were similar in all groups. The relationship between the elastic modulus, E

203   and SM/CT ratio (figure 3C) for these groups shows that stiffness increased as the proportion of

204   connective tissue also increased, note the CT/SM ratio is inverted compared to figure 2B.

205   *Intracellular Ca^{2+} regulation*. It is unclear from the contractile data if reduction of contractile

206   function from exstrophy patients was in part due to reduced contractile function of individual

11

207   myocytes, as well as reduced smooth muscle content. Altered detrusor function was tested by

208   measuring the change of intracellular calcium ($[Ca^{2+}]_i$), in isolated myocytes from normal and

209   exstrophy bladders in response to contractile agonists. $[Ca^{2+}]_i$ was measured in myocytes from

210   cloacal exstrophy bladders, but the small number of cells precluded statistical comparison, but data

211   are shown for comparison. Data from the two paediatric exstrophy groups have been combined as

212   myocytes were isolated from a total of only seven samples (n=3, 4 from young and older paediatric

213   exstrophy groups). The resting $[Ca^{2+}]_i$ was similar in myocytes from the remaining groups (Table 2).

214   The changes of $[Ca^{2+}]_i$, $\Delta[Ca^{2+}]_i$, in response to four contractile interventions were recorded:

215   carbachol for muscarinic receptor activation; ABMA for purinergic receptor activation; 80 mM

216   extracellular KCl to depolarise the cell and activate Ca^{2+} channels; caffeine to release Ca^{2+} from

217   intracellular stores. With cells from control bladder samples the rise of $[Ca^{2+}]_i$, $\Delta[Ca^{2+}]_i$, was not

218   significantly different for all interventions. Moreover, $\Delta[Ca^{2+}]_i$ for each intervention was similar in

219   myocytes from paediatric and neonatal exstrophy bladders (Table 2).

220   *Quantitative image intensity analysis*. Multichannel immunofluorescence labelling of a normal and

221   paediatric exstrophy samples (figure 4A, parts a, c), along with higher power regions (parts b, d)

222   presented as deconvoluted images, were used for quantitative analysis. Data from nine normal

223   bladder samples and seven exstrophy (five paediatric and two neonatal exstrophy) are shown

224   (figure 4B). The intensity measurements of the different immunolabels demonstrated a reduction

225   of MMP-7 signal (p=0.045), and more significant reductions of β−catenin (p=0.0037) and *c*-myc

226   (p<0.001) in the exstrophy samples; there was no change to cyclin-D1 labelling.

Discussion

Exstrophy and detrusor function. Reduction of the SM/CT ratio in human exstrophy detrusor correlates with similar previous findings [7,8]. The reduced ratio was greatest in neonates with bladder and cloacal exstrophy, with evidence of recovery in older children of the two paediatric exstrophy groups. Recovery of smooth muscle relates either to the closure procedure and/or ageing itself. As the SM/CT ratio reduced, the greater was reduced contractile function, whether elicited by smooth muscle agonists or electrical stimulation of embedded motor nerves. The ratio of force generated either by nerve-mediated stimulation or carbachol exposure was similar in normal and exstrophy cohorts, suggesting detrusor muscle motor innervation itself was not affected by exstrophy. Moreover, there is no detriment to intracellular signalling pathways that regulate intracellular $[Ca^{2+}]$ between the normal and exstrophy groups, as tested by receptor agonists, cell depolarisation (high-K) or intracellular Ca^{2+} release (caffeine). These data confirm previous observations of exstrophy myocytes responding to carbachol and high-K solutions [15], although the reduced basal $[Ca^{2+}]$ in their exstrophy myocytes was not observed here. Thus, in combination with the histological differences in SM/CT content, replacement of smooth muscle with connective tissue is the most likely reason for reduced active force development. Maintained myocyte function with exstrophy is also indicated by similar motility and proliferation in response to growth factors [16].

Another consequence of the increased connective tissue content in exstrophy bladder samples was greater passive stiffness; the SM/CT ratio showed an inverse relationship to passive stiffness. We did not determine the collagen subtype, which is a major component of connective tissue. However, previous work with adult bladder samples has shown that excessive collagen deposition and poorly compliant bladders is associated with a shift from type-I to type-III collagen [17]. The *in vitro* change to a stiffer, less contractile phenotype is consistent with some clinical studies [18]. Moreover, attempts to improve bladder contractile performance with inotropic agents would be less successful

13

251 as residual muscle properties are unaltered. Increased connective tissue, associated with reduced

252 metalloproteinase expression and increased expression of tissue inhibitors of metalloproteinases

253 (TIMP) is associated with adult bladder outlet obstruction [19,20], or even raised intravesicular

254 pressures [21]. This suggests decreased expression of enzymes that degrade collagen may

255 contribute to a similar situation in bladder exstrophy. Treatment of post-radiation fibrotic bladders

256 with relaxin reduced connective tissue deposition and recovered cystometric function [22] and this

257 may offer a similar treatment option with bladder exstrophy.

258 *Pathways influencing connective tissue deposition*. The *Wnt* pathway, with intracellular Ca^{2+} and

259 transcription factor co-activators as signal transducers, are key in tissue and organ development

260 [23-25]. In particular, *Wnt*-signalling pathways are important in the terminal differentiation of

261 fibroblasts, smooth muscle cells and epithelial cells to collagen-secreting myofibroblasts. There is

262 little work concerned with human neonatal bladder disorders, but genome expression and genome-

263 wide expression studies have implicated changes to *Wnt* signalling pathways in exstrophy [26,27].

264 Quantitative image intensity analysis showed reduced labelling for β-catenin and *c*-myc, with

265 reduction of the matrix-metalloproteinase, MMP-7. However, expression of cyclin-D1, another

266 target of β-catenin transcription was not significantly altered in exstrophy samples. Little is known

267 about the particular *Wnt*-proteins that regulate normal human bladder development and

268 generation of fibrosis, but down-regulation of Wnt11 is associated with fibrosis in patients with

269 bladder pain syndrome [28]. Overall, downregulation of a *Wnt*-related pathway in a congenital

270 bladder anomaly is a novel observation [29] and may result in increased differentiation into

271 fibroblasts rather than a smooth muscle lineage. Future work targetting molecular signalling

272 pathways such as *Wnt* and TGF-β, which likely underpin this developmental disease, has the

273 potential to develop prognostic and therapeutic targets.

274 *Limitations*. Sample availability was limited by the rarity of these conditions and complexity of

275 surgical procedures and statistical analyses were not always possible, especially with the cloacal

276 exstrophy group. It would have been preferable to perform histological, biomechanical and

277 functional studies on each preparation, but in most cases this was not possible. All samples were

278 given an anonymising study code, but researchers were unblinded for functional experiments, as

279 they also retrieved samples. However, histology and immunohistochemistry experiments were

280 undertaken later with researchers now blinded; the code and diagnosis was revealed only after data

281 collection.

282 **Conclusion**

283 This study highlights the critical importance of raised connective tissue content in bladder

284 exstrophy. Exstrophy management has dramatically improved and surgery now provides continence

285 and urethral voiding for many. However, some still fail to achieve continence and the development

286 of therapies is important. Reduced detrusor contractile function with exstrophy is highly correlated

287 with the SM/CT ratio, alongside normal myocyte function. We suggest a molecular explanation for

288 increased CT in terms of reduced *Wnt*-pathway function.

289 **Funding**

290

293

294 **References**

295 [1]   Jayachandran D, Bythell M, Platt MW, et al. Register based study of bladder exstrophy-

296 epispadias complex: prevalence, associated anomalies, prenatal diagnosis and survival. J Urol 2011;

297 186: 2056-2060.

298   [2]   Kelly JH. Vesical exstrophy: repair using radical mobilisation of soft tissues. Pediatr Surg Int

299   1995; 10: 298–304

300   [3]   Woodhouse CR, Redgrave NG. Late failure of the reconstructed exstrophy bladder. BJU Int

301   1996; 77: 590–592.

302   [4]   Cuckow P, Desai D, Ryan K. Physiological reconstruction of the lower urinary tract in bladder

303   exstrophy - 10 years' experience with the Kelly operation. J Urol 2010; 183: e210.

304   [5]   Borer JG, Starkosha R, Bauer SB, et al. Combined cystometrography and electromyography of

305   the external urethral sphincter following complete primary repair of bladder exstrophy. J Urol 2014;

306   191: 1547-1552.

307   [6]   Lee BR, Perlman EJ, Partin AW, et al. Evaluation of smooth muscle and collagen subtypes in

308   normal newborns and those with bladder exstrophy. J Urol 1996; 156: 2034-2036.

309   [7]   Slaughenhoupt BL, Mathews RI, Peppas DS, et al. A large animal model of bladder exstrophy:

310   observations of bladder smooth muscle and collagen content. J Urol 1999; 162: 2119-2122.

311   [8]   Mathews R, Wills M, Perlman E, et al. Neural innervation of the newborn exstrophic bladder:

312   an immunohistochemical study. J Urol 1999; 162: 506-508.

313   [9]   Kendall RT, Feghali-Bostwick CA. Fibroblasts in fibrosis: novel roles and mediators. Front

314   Pharmacol 2014; 5: 1-13.

315   [10] Yang L, Liu R, Wang X, et al. Imbalance between matrix metalloproteinase-1 (MMP-1) and

316   tissue inhibitor of metalloproteinase-1 (TIMP-1) contributes to bladder compliance changes in

317   rabbits with partial bladder outlet obstruction (PBOO). BJU Int. 2013; 112: E391-397.

318   [11] Xu L, Cui WH, Zhou WC, et al. Activation of Wnt/β-catenin signalling is required for TGF-

319   β/Smad2/3 signalling during myofibroblast proliferation. J Cell Mol Med 2017; 21: 1545-1554.

320   [12] Körberg IB, Hofmeister W, Markljung, E et al. Wnt3 involvement in human bladder exstrophy

321   and cloaca development in zebrafish. Hum Mol Gen 2015; 24: 5069-5078.

322 [13] Sui G, Fry CH, Malone-Lee J, et al. Aberrant Ca^{2+} oscillations in smooth muscle cells from

323 overactive human bladders. Cell Calcium 2009; 45: 456-464.

324 [14] Arya M, Thrasivoulou C, Henrique R, et al. Targets of wnt/ß-catenin transcription in penile

325 carcinoma. PloS one 2015; 10: p.e0124395.

326   [15] Suson KD, Stec AA, Shimosa LA, Gearhart JP. Initial characterization of exstrophy bladder

327 smooth muscle cells in culture. J Urol 2012; 188: 1521-1527.

328 [16] Suson KD, Stec AA, Gearhart JP, Shimosa LA. Transforming growth factor-β1 mediates

329 migration

330 [17] Imamura M, Kanematsu A, Yamamoto S, et al. Basic fibroblast growth factor modulates

331 proliferation and collagen expression in urinary bladder smooth muscle cells. Am J Physiol Renal

332 Physiol 2007; 293: F1007-1017.

333 [18] Puri A, Mishra K, Sikdar S, et al. Vesical preservation in patients with late bladder exstrophy

334 referral: histological insights into functional outcome. J Urol 2014: 192: 1208-1214.

335 [19] Peters CA, Freeman MR, Fernandez CA, et al. Dysregulated proteolytic balance as the basis of

336 excess extracellular matrix in fibrotic disease. Am J Physiol 1997; 272: R1960-1965.

337 [20] Yang L, Liu R, Wang X, et al. Imbalance between matrix metalloproteinase-1 (MMP-1) and

338 tissue inhibitor of metalloproteinase-1 (TIMP-1) contributes to bladder compliance changes in

339 rabbits with partial bladder outlet obstruction (PBOO). BJU Int 2013; 112: e391-397.

340 [21] Backhaus BO, Kaefer M, Haberstroh KM, et al. Alterations in the molecular determinants of

341 bladder compliance at hydrostatic pressures less than 40 cm H_2O. J Urol 2002; 168: 2600-2604.

342 [22] Ikeda Y, Zabbarova IV, Birder LA et al. Relaxin-2 therapy reverses radiation-induced fibrosis

343 and restores bladder function in mice. Neurourol Urodyn 2018 May 28. doi: 10.1002/nau.23721

344 [23] Semenov MV, Habas R, Macdonald BT, et al. SnapShot: noncanonical Wnt signaling pathways.

345 Cell 2007; 131: 1378.e1-1378.e2

346 [24] Sugimura R, Li L.   Noncanonical Wnt signaling in vertebrate development, stem cells, and

347 diseases. Birth Defects Res C Embryo Today 2010; 90: 243-256.

348 [25] Thrasivoulou C, Millar M, Ahmed A. Activation of intracellular calcium by multiple Wnt ligands

349 and translocation of ß-catenin into the nucleus: a convergent model of Wnt/Ca^{2+} and Wnt/ß-catenin

350 pathways. J Biol Chem 2013; 288: 35651-35659.

351 [26] Qi L, Chen K, Hur DJ et al.   Genome-wide expression profiling of urinary bladder implicates

352 desmosomal and cytoskeletal dysregulation in the bladder exstrophy-epispadias complex. Int J Mol

353 Med; 27: 755-765.

354 [27] Draaken M, Knapp M, Pennimpede T et al. Genome-wide association study and meta-analysis

355 identify ISL1 as genome-wide significant susceptibility gene for bladder exstrophy. Plos Genetics

356 2015; 11(3): e1005024.

357 [28] Choi D, Han JY, Shin JH, et al. Downregulation of WNT11 is associated with bladder tissue

358 fibrosis in patients with interstitial cystitis/bladder pain syndrome without Hunner lesion. Sci Rep

359 2018; 8: 9782.

360 [29]   Halt K, Vainio S. Coordination of kidney organogenesis by Wnt signalling. Pediatr Nephrol

361 2014; 29: 737-744.

362 **Figure legends**

363 Figure 1. **Smooth muscle and connective tissue in normal and exstrophy bladders**. A: van Gieson

364 stain of detrusor samples from normal (upper) and paediatric exstrophy (lower) bladders: orange

365 smooth muscle; red connective tissue. B: The smooth muscle:connective tissue (SM/CT) ratio of the

366 detrusor layer from normal, and the four exstrophy cohorts, ***$p<0.001$
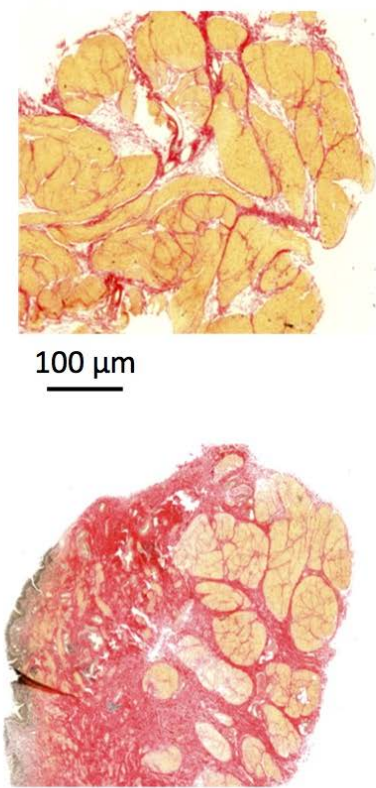
367 Figure 2. **Active contractile properties of detrusor from normal and exstrophy bladders.** A: Force-

368 frequency curves of nerve-mediated contractions from control and young and old paediatric (paed),

369 neonatal (neo) and cloacal (cloa) exstrophy bladders. Estimation of $T_{max,n-m}$ and $f_{1/2}$ values are

370 shown for the control bladder curve. B. The association between the SM/CT ratio and either the

371 T_{max} for nerve-mediated contractions ($T_{max,n-m}$, open circles) or for maximum carbachol contractions

372 ($T_{max,carb}$, closed circles).

373 Figure 3. **Biomechanical characteristics of detrusor from normal and exstrophy bladders.** A:

374 Tracing of isometric force for a stretch of 1 mm for 50 s, resting muscle length 5 mm. B: values of

375 elastic modulus, *E,* for samples from normal, paediatric exstrophy and neonatal exstrophy bladders.

376 ***$p<0.001$ *vs* normal, ### $p<0.001$ paediatric *vs* neonatal exstrophy. C: the association between

377 the CT/SM ratio and elastic modulus, *E*, for samples from control, paediatric exstrophy and neonatal

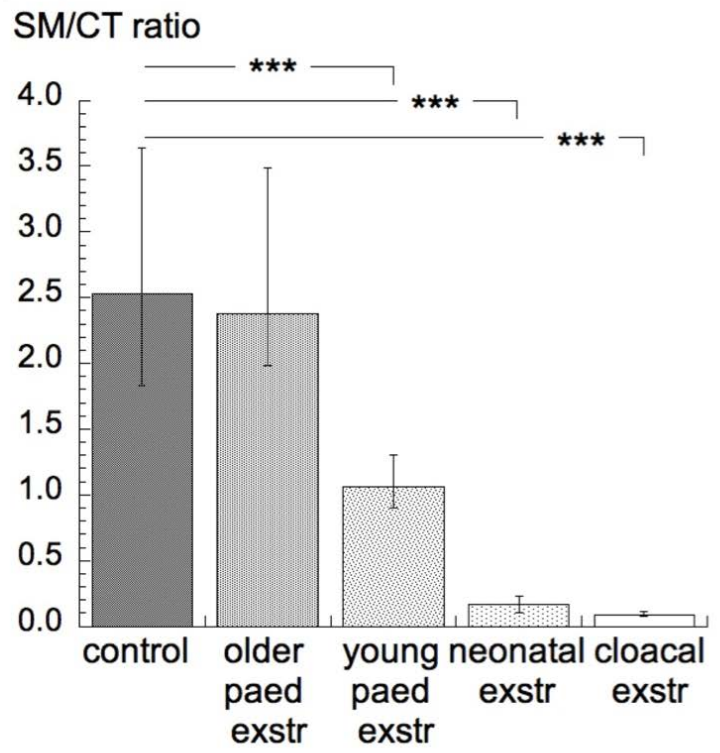378 exstrophy bladders. Note logarithmic axes in parts B and C.

379 Figure 4. **Quantitative analysis of *wnt*-related proteins**. A: Representative images (x63) of normal

380 (left) and paediatric exstrophy (right) detrusor. Images a and c: composite overlay of four

381 fluorphores: Cy3 (yellow) for MMP-7; Cy5 (purple) for cyclin-D1; FITC (green) for β-catenin; Cy3.5

382 (red) for *c-myc*; DAPI nuclear label (blue). Images b,d: higher magnification regions sections to show

383 more clearly individual colour labels B: Quantitative analysis of expression of the four epitopes

384 carried out on grey constructs of images filtered for the four fluorochromes. Median data [25,75%

385 interquartiles], *$p<0.05$, **$p<0.01$, ***$p<0.001$, (N=9;7: control; exstrophy).
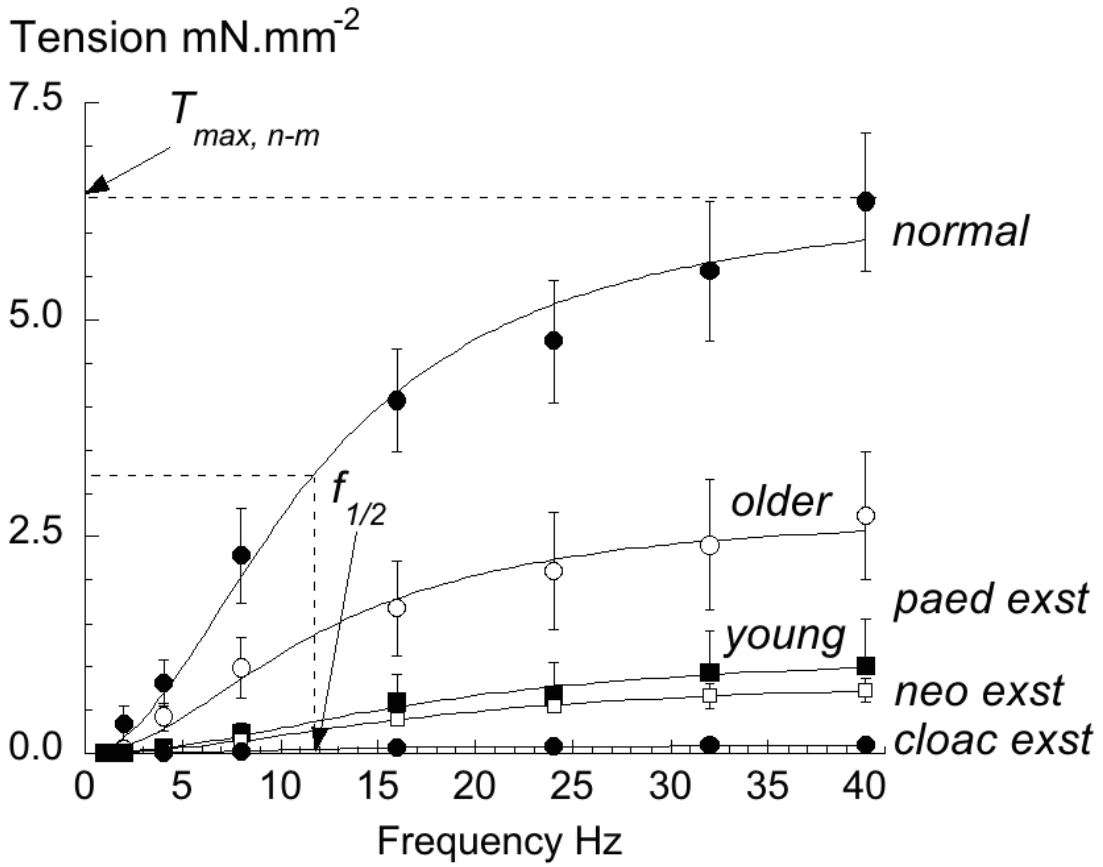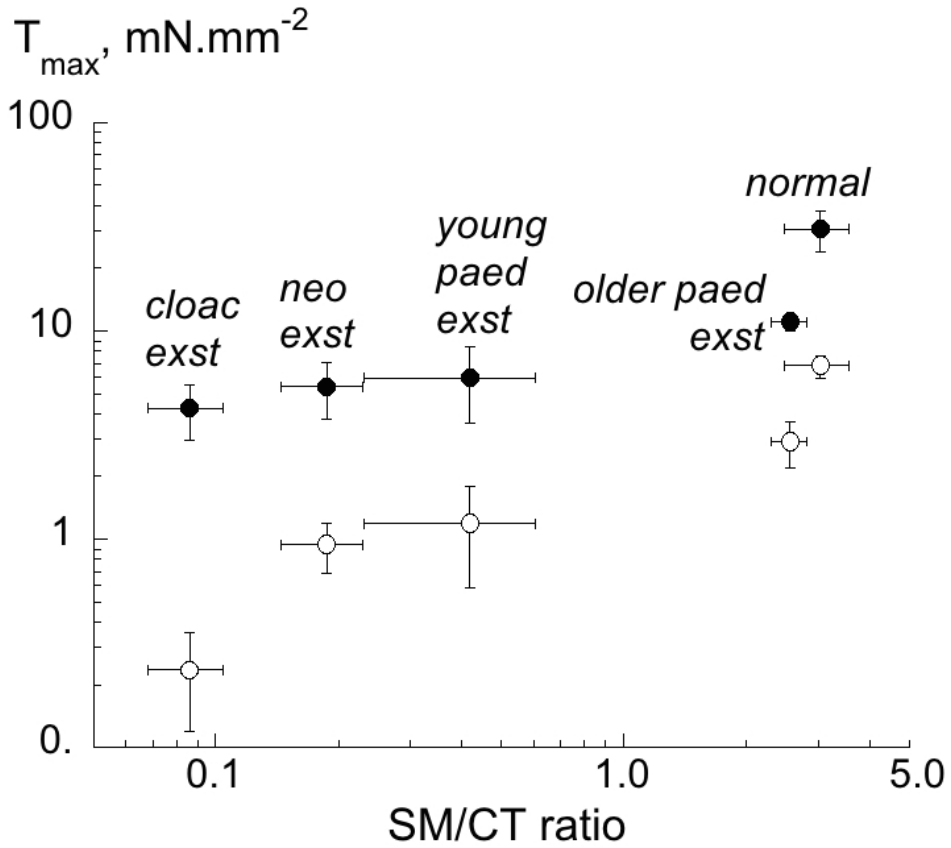
386   Figure 1

A

100 μm

B

SM/CT ratio

387
388

389   Figure 2

A

Tension mN.mm^{-2}

$T_{max,\ n-m}$

$f_{1/2}$

normal

older

paed exst

young

neo exst

cloac exst

Frequency Hz

B

T_{max}, mN.mm^{-2}

normal

cloac exst

neo exst

young paed exst

older paed exst

SM/CT ratio

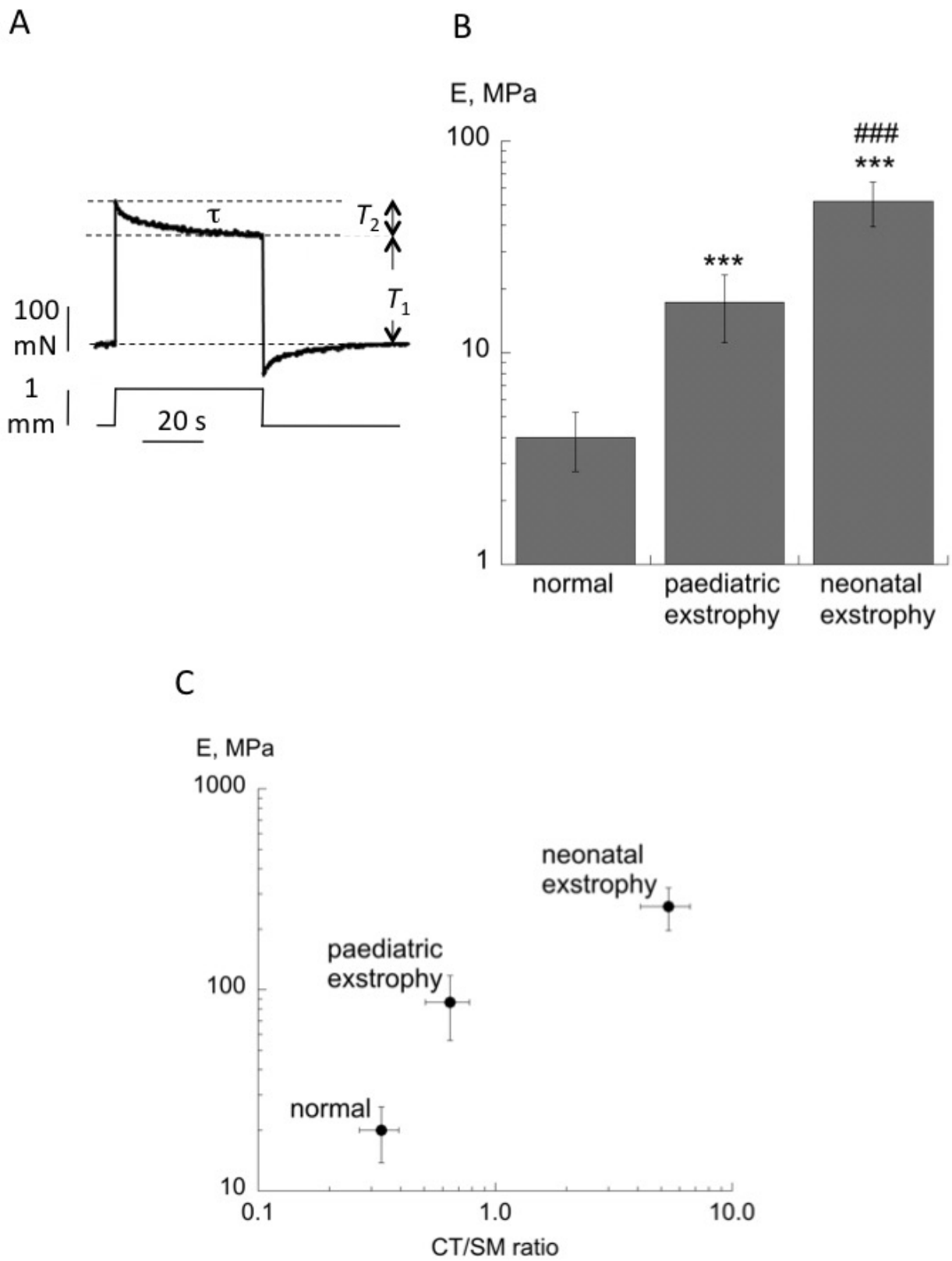391   Figure 3

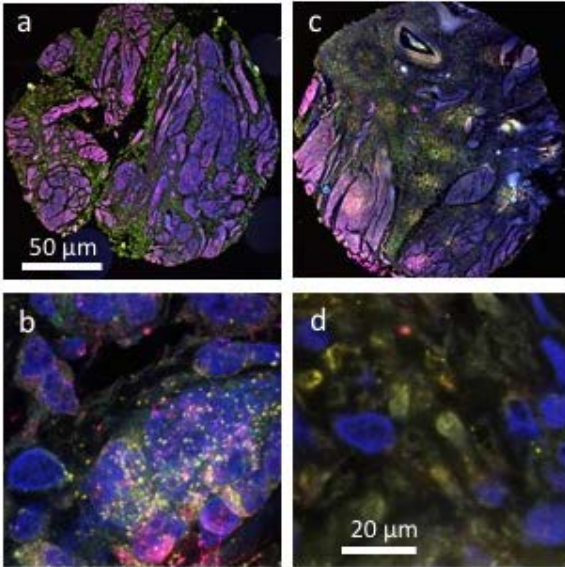392
393

394   Figure 4

A

B

signal intensity (x10^8)
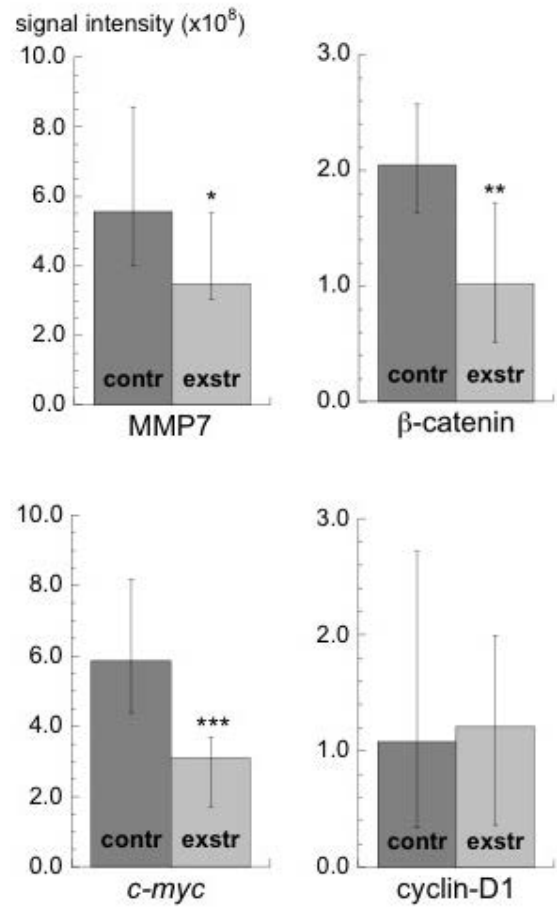

395
396

Table 1. Smooth muscle (SM): connective tissue (CT) ratios and contractile characteristics in detrusor muscle from normal and exstrophy bladders. The paediatric exstrophy data is shown as two sets; from older and younger children (see Methods). Mean data ±SEM (*N* biopsy samples). *p<0.05; **p<0.01; ***p<0.001 *vs* normal.

	Normal	Older Paediatric exstrophy	Young Paediatric exstrophy	Neonatal exstrophy	Cloacal exstrophy
Histology					
SM/CT ratio	3.03±0.56 (11)	2.56±0.26 (6)	0.42±0.19 (10)***	0.19±0.042 (5)***	0.086±0.018 ( )***
Contractile data					
$T_{max,n-m}$, mN.mm^{-2}	6.80±0.86 (10)	2.93±0.75 (6)*	1.19±0.60 (11)**	0.93±0.25 (5)***	0.24±0.12 (7)***
$f_{1/2}$, Hz	13.2±2.1 (10)	14.2±3.6 (6)	19.4±3.5 (11)	17.2±3.9 (5)	15.6±1.0 (7)
Atropine resist	60.0±28.3 (7)	51.2±14.1 (6)	26.1±8.7 (7)	26.7±17.5 (5)	ND
$T_{max,carb}$ mN.mm^{-2}	30.8±6.68 (10)	11.0±1.01 (6) **	5.98±2.40 (10)***	5.41±1.63 (5)***	4.25, 1.06 (2)
Carb pEC_{50}	5.51±0.04 (10)	6.28±0.12 (6)**	5.99±0.12 (10)**	5.75±0.64 [(5)*	5.67, 5.70 (2)
T_{ABMA}, mN.mm^{-2}	11.2±2.68 (7)	2.02±0.54 (6)***	1.69±0.50 (11)***	0.94±0.22 (5)***	0.05±0.01 (3)
$T_{max,n-m}/T_{max,carb}$	0.44±0.11 (10)	0.24±0.04 (6)	0.34±0.10 (10)	0.20±0.08 (5)	ND

Table 2.   Biomechanics and intracellular [Ca^{2+}] data in detrusor muscle from normal and exstrophy bladders.   The paediatric exstrophy data are shown as one data set.   Mean data ±SEM (*n* preparations from *N* biopsy samples).   *p<0.05.   *E*, elastic modulus is used as a measure of detrusor stiffness. E_2 is the viscoelastic component of instantaneous stiffness – see Methods for details.

	Normal	Paediatric exstrophy	Neonatal exstrophy	Cloacal exstrophy
Biomechanics data				
E, MPa (elastic modulus)	20.0±6.20 (9)	86.5±28.1 (6)*	259±61.5 (4)*	
E_2, MPa	6.75±3.60 (9)	20.2±6.60 (6)*	96.0±62.1 (4)*	
τ, seconds	9.6±1.4 (9)	10.8±0.6 (6)	10.4±0.5 (4)	
Intracell [Ca^{2+}] data				
Resting [Ca^{2+}]$_i$, nM	75±16 (9)	111±23 (7)	116±20 (4)	83±9 (3)
Δ[Ca^{2+}]$_i$ carb, nM	416±100 (9)	432±128 (7)	413±125 (4)	70±12 (3)
Δ[Ca^{2+}]$_i$ ABMA, nM	361±101 (9)	561±150 (7)	401±65 (4)	118±52 (3)
Δ[Ca^{2+}]$_i$ KCl, nM	322±94 (9)	419±109 (7)	337±123 (4)	106±37 (3)
Δ[Ca^{2+}]$_i$ caff, nM	401±120 (4)	469±102 (6)	394±119 (4)	91,171 (2)